Engineering Structures 167 (2018) 121–131

Contents lists available at ScienceDirect

Engineering Structures

journal homepage: www.elsevier.com/locate/engstruct

Deterioration of cracks in onshore wind turbine foundations

Jack McAlorum[a,*], Marcus Perry[b], Grzegorz Fusiek[a], Pawel Niewczas[a], Iain McKeeman[a], Tim Rubert[a]

[a] Department of Electronic and Electrical Engineering, University of Strathclyde, Glasgow G1 1XW, UK
[b] Department of Civil and Environmental Engineering, University of Strathclyde, Glasgow G1 1XJ, UK

ARTICLE INFO

Keywords:
Cracks
Foundations
Degradation
Fibre-optic
Strain
Deterioration

ABSTRACT

Cracks can occur in reinforced-concrete onshore wind turbine foundations due to factors such as the use of substandard concrete mix, mistakes in foundation design or multi-stage concrete pouring under challenging weather conditions. Cracks are routinely identified via above ground inspections and follow-on examination of excavated underground surfaces and are repaired, for example with resin injection and grouting. Their impact on the structure or the efficacy of the repair are often unknown as crack degradation during normal operating conditions is unexplored. In this work, sub-surface cracks in an onshore wind turbine foundation have been instrumented with fibre-optic based strain sensors in an attempt to determine severity and magnitude of deterioration over time. Here we determine cracks monitored show a small magnitude of deterioration over the initial 9-month period after sensor installation, suggesting that repair is not required. We propose a novel methodology for the classification of the types of deterioration evident in cracks as "reactive", "permanent" and "behavioural", and demonstrate methods to extract these types of deterioration. Such methods will continually be developed over time as further knowledge of crack behaviour is gained to determine appropriate limits and identify the optimal time to repair.

1. Introduction

Onshore wind turbines are becoming a focus of structural health monitoring (SHM), due to their hugely increasing role in renewable energy generation. As of 2017, onshore wind energy makes up 22.5% of the world's renewable capacity [1,2]. Extending the life of these assets, or even ensuring they reach their design life is vital for the continued investment and maximisation of environmental benefits. To date, mostly the mechanical moving systems (gearbox, generator) are instrumented, likely due to the higher failure rate [3,4]. Other implementations focus on dynamical strain behaviour in the tower or blades, analysing the fatigue damage [5,6]. Support structures (usually gravity-based, reinforced concrete foundations) are the least monitored part of an onshore wind turbine despite being safety critical structures. Cracking of the concrete is of primary concern, as water ingress can cause corrosion to the steel reinforcement. This warrants the monitoring of any cracks in onshore wind turbine foundations to ensure an irreversible state is not reached.

Cracks appear in other reinforced concrete structures, however, SHM sensor systems are not always applied post-damage. Generally, SHM involves monitoring structural loading using sensor systems such as accelerometers or strain gauges. These structures exist in urban, public or transport infrastructure [7–9], the oil and gas industry [10] and aerospace [11]. Sensors have replaced the conventional manual inspection for SHM as they provide benefits such as: measurement of sub-surface damage [12], potentially less expensive long term cost and continual uninterrupted accurate measurements. One such application for SHM sensor systems is damage detection [13–15]. Cracks in concrete are usually repaired immediately without further severity analysis. There is also the possibility that cracks reappear over the repaired section, as these locations are usually of weakest structural integrity or highest loading. This can cause increased costs in the long term.

All of the aforementioned SHM systems focus on monitoring characteristics such as structural strains, vibrations, wind speed, temperature, displacements and crack initiation; damage degradation is not always the primary concern. Monitoring damage degradation could provide a more informative description of the structure's health and ensure damage is fixed at the optimal time, avoiding the unrequired long term costs of repairing damage of low severity.

The main concern with foundation cracking is that a more extensive network of wide cracks can increase the likelihood of corrosive and detrimental agents such as moisture, chlorides and sulphates penetrating concrete and reaching steel. Not all cracks will affect a structures integrity, however it is this corresponding likelihood that

* Corresponding author.
E-mail address: jack.mcalorum@strath.ac.uk (J. McAlorum).

https://doi.org/10.1016/j.engstruct.2018.04.003
Received 11 September 2017; Received in revised form 26 February 2018; Accepted 3 April 2018

increases the overall risk. Thorough assessment may be required prior to sensor installation to determine if cracks are appropriate to measure, which may include evidence from manual inspection that cracks show opening over time. Combining this - damage progression monitoring to onshore wind turbine support structures may provide a more effective way to monitor the health of onshore wind turbine foundations. One example of this has been carried out on an onshore wind turbine embedded can foundation design by Currie et al. [16]. The damage witnessed was at the can-foundation interface, and is therefore specific to this foundation design.

In this work, the objective is to monitor cracks witnessed on the face of an onshore wind turbine gravity foundation to investigate the rate of degradation. Optical sensors known as fibre Bragg gratings (FBGs) were utilized in this study due to the range of advantages they possess. These include: immunity to electromagnetic interference, multiplexing ability, small size, robustness, and long-life capability [17–19]. Ko et al. [8] replaced the electrical accelerometers in a bridge load monitoring system with FBGs due to these benefits [20]. Some FBG systems have also been implemented to detect the onset of damage in structures [13], where sensors were placed along points of highest loading, allowing eventual damage initiation to be detected. Sensor installation and verification is reported in [21]. In the following, cracks are analysed for deterioration over the initial 9 months of monitoring. Although loading will be directly related to turbine operation, such a system could be adopted for any type of concrete structure exhibiting cracks.

This paper is structured as follows: Section 2 provides an overview of the sensor design, installation and description of the strain extraction equations. Section 3 provides a brief description of the wind turbine loading model (explained in detail in [21]) and extrapolation of the tower strains to crack displacements. Section 4 outlines the results found over the initial 9-month period, defining the types of deterioration and methods to extract them. A discussion is then presented in Section 5 including an outline of the planned future work. Finally, a conclusion is provided in Section 6.

2. Sensors

2.1. Fibre Bragg gratings

FBGs have been used to measure a variety of physical quantities including strain, displacement, temperature, pressure, and current [22,23]. Ultra violet light of modulating intensity is used to create a periodic alteration of the refractive index in an optical fibre, establishing the Bragg grating. Broadband light incident on said FBG incites a narrow band reflection centered around the Bragg wavelength peak, λ_b, measured and saved using an interrogator system (Fig. 1). This peak wavelength is shifted for a bonded FBG by temperature change, ΔT, and any applied linear strain, ϵ_z, shown in Eq. (1):

$$\frac{\Delta\lambda_b}{\lambda_b} = K_T \Delta T + K_\epsilon \, \epsilon_z \tag{1}$$

here K_T and K_ϵ are the temperature and strain sensitivities of the FBG

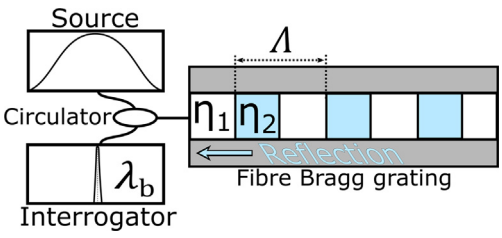

Fig. 1. FBG operation: broadband source guided through FBG causes reflection of a narrow band of wavelengths, the peak of which is centered around Bragg wavelength λ_b. The value of λ_b is dependent on the modulation between refractive indices η_1 and η_2, and grating period Λ.

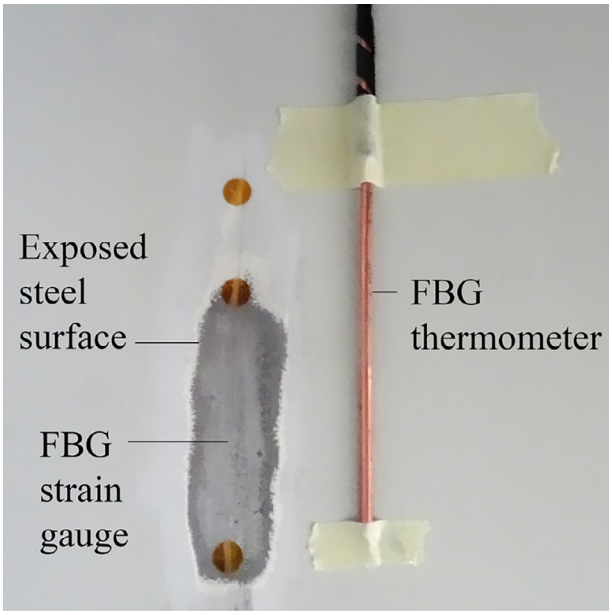

Fig. 2. Tower Module: strain FBG is epoxied to tower wall, with temperature FBG isolated [21].

respectively. An unboned FBG temperature sensor ($K_\epsilon = 0$), multiplexed to and in thermal contact with the strain FBG, is used to perform compensation. The FBG temperature sensor design is described in [24]. Using this, we can extract the temperature compensated linear strain, ϵ_z, applied to the bonded FBG.

2.2. Tower modules

Tower sensor modules consisted of one bonded FBG and one unbonded FBG thermometer, as shown in Fig. 2. A total of four of these modules were installed within the tower, 50 cm above ground level. Locations were chosen relative to the known prevailing wind direction, to allow monitoring of the overturning moment strains. An octagonal gravity-based slab foundation is illustrated in Fig. 3, labelled with sensor locations and direction of prevailing wind.

2.3. Foundation modules

The locations of the unique cracks monitored in this study are shown in Fig. 3. Foundations of this type, with multiple-stage concrete pouring are prone to crack initiation between plinth-rib interface. Over time, due to issues with steel reinforcement design combined with continuous dynamic loading, these cracks can develop and widen. In this case, the cracks have propagated to the face of the plinth (as illustrated in Fig. 3). Previous excavation campaigns carried out by the turbine operator have provided evidence that these cracks do open over time. The current method for repair is grout-injection, which involves using pressurised or jet equipment to fill the void with grout in order to strengthen the section or reduce ingress. From supervisory control and data acquisition (SCADA) data, the mean wind speed during the monitoring period considered in this work is $\approx 5.67\ \mathrm{ms}^{-1}$, suggesting conditions at this site are temperate.

One particular face crack monitored is shown in Fig. 4. Plinth and face cracks prior to sensor installation are shown in Fig. 5. Monitoring crack widening is imperative, as width is directly related to penetration depth [25], and water or chloride reaching steel can cause corrosion. Monitoring cracks over the long-term, notifying if specific limits are reached, will allow understanding of the foundations health and allow maintenance to take place at optimal times.

Monitored cracks were chosen based on a number of factors, the

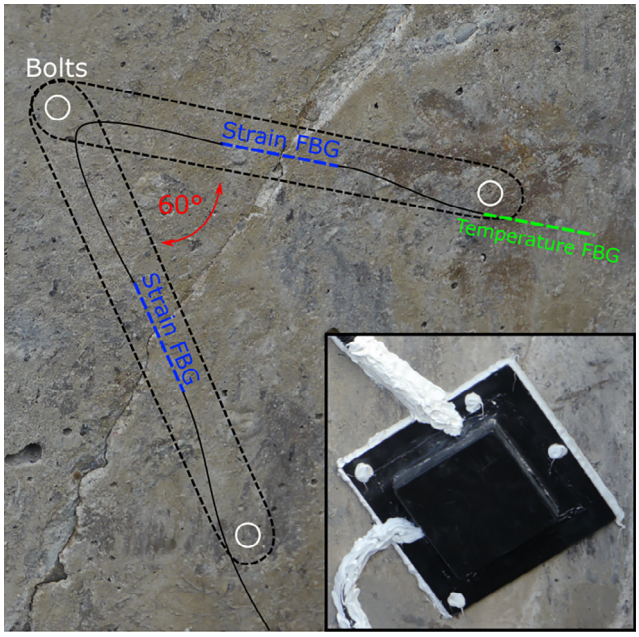

Fig. 3. Octagonal slab foundation: all sensor locations relative to predominant wind direction. Analysed sensor modules "B" and "C" are identified. Labelled rib is cut for illustrative purposes only.

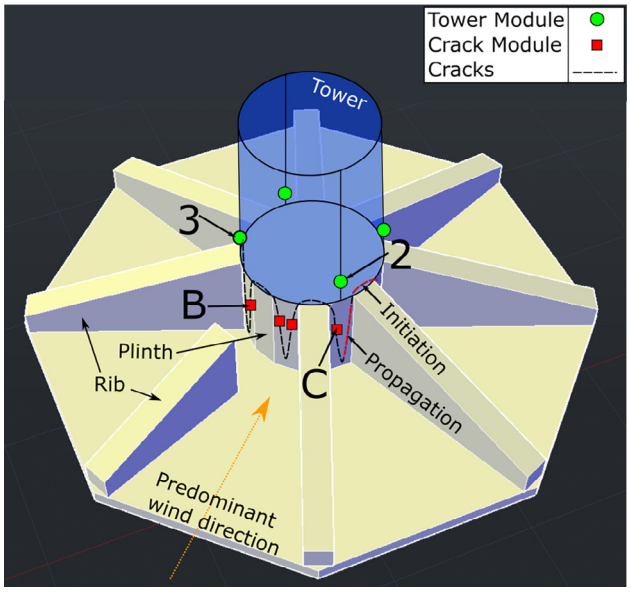

Fig. 4. Foundation Module: two strain FBGs are epoxied to steel arms at a 60° angle, with temperature FBG isolated. Insert: protective housing of sensor module, with silicon applied.

most important one was crack's visible severity. As expected, the most severe cracks (identified in Fig. 3 by crack module locations) were discovered on faces closest to the predominant wind direction [21]. This is most likely induced by the overturning moment causing these faces to be in tension, opening the cracks. Using this information, a correlation should be evident between crack width and overturning moment, and hence wind speed. However, due to unknown quantities such as the crack depth and any sub-surface networks, this exact relationship is challenging to define. This will be explored further in Section 3.

Foundation modules consisted of two epoxied strain monitoring FBGs and one temperature monitoring FBG, depicted in Fig. 4. Two carbon-steel arms were brazed together at a 60° angle with a bolt

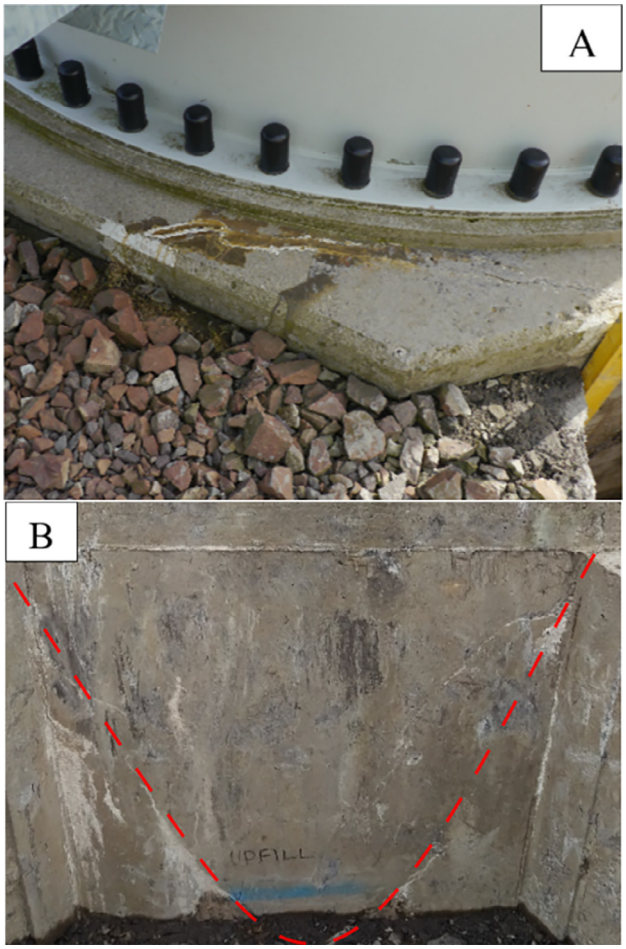

Fig. 5. Visible cracks on foundations; A: along plinth B: 'U' shape face cracks.

intersecting, following which the strain FBGs were epoxied to the centre of the arms. This bidirectional strain measurement allows the possibility for tearing crack movements to be extracted [26]. Four modules were fit over four face cracks deemed most severe and appropriate to monitor, located closest to the predominant wind direction (Fig. 3). For referencing purposes, each sensor is labelled by module letter and number (for example, module B contains crack sensors B1 and B2).

Short-gauge FBG sensors can effectively measure the strain at the centre of the steel arms. Long-gauge sensors are required to monitor large, irregular cracks due to the inhomogeneous nature of concrete [27]. The strain in the steel arms is described by [27]:

$$\epsilon_z = \frac{\Delta L_a}{L_a} = \frac{1}{L_a}\int_{x_A}^{x_B} \epsilon_c(x)dx + W_c \tag{2}$$

where ΔL_a is the change in displacement between anchorage points $x_{A,B}$ of the steel arm with length, $L_a = 10$ cm representing the distance between. This displacement change is caused by surface strains or existing crack displacements. The W_c term represents propagation discontinuities due to new cracks or inclusions in the concrete [27]. The integral shows that the strain measured is an average between the anchorage points. FBGs measure ϵ_z, which is the linear strain in the steel arm found from Eq. (1).

Cracks have three primary modes of displacement: mode I (crack opening), mode II (sliding) and mode III (tearing) as described in [28], which have been illustrated in Fig. 6 window A. Eq. (3) shows the sum of strains for these displacements evident in sensors in this work:

$$\epsilon_z = \epsilon_l + \epsilon_t \tag{3}$$

where mode I and II (opening and sliding respectively) are summed in

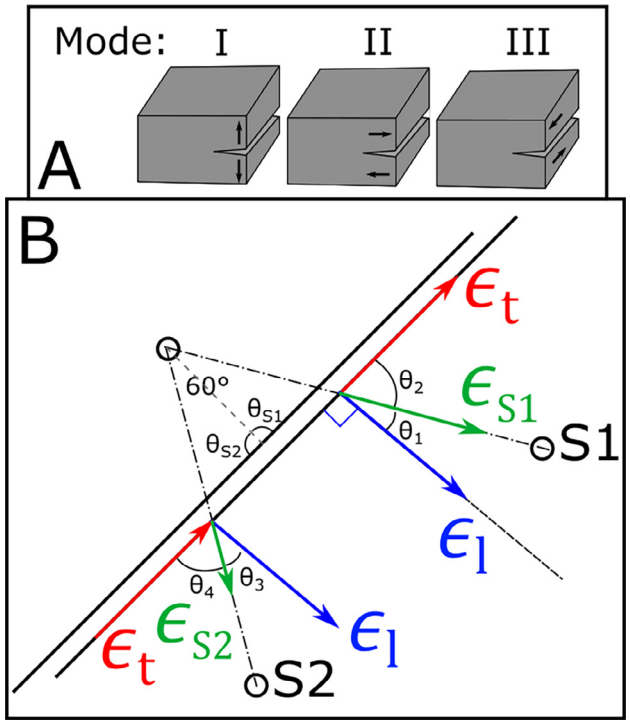

Fig. 6. Window A: diagram depicting crack modes. Window B: applying trigonometry to extract strain caused by tearing displacement mode III (Eqs. (4) and (5)).

the linear crack strain term ϵ_l and mode III (tearing) is represented by ϵ_t. The sensor in this work is unable to differentiate mode I from mode II, it is expected that mode II will be negligible and mode I will dominate. A fourth potential crack mode includes the rotation of faces surrounding cracks, however, this will also be dominated by mode I displacements and has thus been neglected. Prior to this work it was decided that these mode II sliding displacements as well as face rotations were not of interest and would be too difficult to extract.

Until this point, it has been assumed that the tearing displacements are also too small to be measured ($\epsilon_t = 0$). The strains and displacements shown represent all types, but are assumed to be dominated only by opening. Crack deterioration could cause ϵ_t to increase. To extract this accurately, a simple trigonometry diagram can be used, shown in Fig. 6 window B.

Ideally, the sensors would be positioned with $\theta_{S1} = \theta_{S2} = 90°$ so that $\theta_1 = \theta_3 = 30°$ and $\theta_2 = \theta_4 = 60°$. Convenient bolt positioning and crack non-uniformity restricted sensor placement during installation, thus the ideal relationship is not applicable. In the case shown in Fig. 6, the tearing strain ϵ_t causes compression on sensor S2 and tension on sensor S1. The linear strain ϵ_l shown causes tension on both sensors. With knowledge of either θ_{S1} or θ_{S2} and total strain from each sensor, we can differentiate linear and tearing strains. Firstly, each sensor can be expressed by Eqs. (4) and (5):

$$\epsilon_{S1} = \epsilon_l \cos\theta_1 + \epsilon_t \cos\theta_2 \tag{4}$$

$$\epsilon_{S2} = \epsilon_l \cos\theta_3 - \epsilon_t \cos\theta_4 \tag{5}$$

where the polarity of the ϵ_t term depends on the tearing displacement occurring. If we assume the case shown in Fig. 6 window B and acquire a negative ϵ_t, the opposite tearing is occurring. Subtracting ϵ_{S2} from ϵ_{S1} and substituting equivalent values of θ_{S1} for each angle acquires:

$$\epsilon_{S1} - \epsilon_{S2} = \epsilon_l \cos(\theta_{S1}) + \epsilon_t \sin(\theta_{S1}) \tag{6}$$

therefore should $\theta_{S1} = 90°$ then the extraction of ϵ_t is the difference in sensor strains. As mentioned, due to complications with bolt positioning this was not possible. In most cases this difference can be used to distinguish if any tearing is occurring. Then, to accurately extract ϵ_t when only ϵ_{S1},ϵ_{S2} and θ_{S1} (or equivalently, θ_{S2}) are known, we rearrange and input the equivalent angles in terms of θ_{S1}:

$$\epsilon_l = \frac{\epsilon_{S1} - \epsilon_t \left(\frac{-\sqrt{3}}{2}\cos(\theta_{S1}) + \frac{1}{2}\sin(\theta_{S1})\right)}{\frac{1}{2}\cos(\theta_{S1}) + \frac{\sqrt{3}}{2}\sin(\theta_{S1})} \tag{7}$$

which can be substituted into Eq. (6) to provide ϵ_t:

$$\epsilon_t = \frac{D(\epsilon_{S1} - \epsilon_{S2}) + \epsilon_{S1}\cos(\theta_{S1})}{-\frac{\sqrt{3}}{2}\cos^2(\theta_{S1}) + \frac{1}{2}\sin(\theta_{S1})\cos(\theta_{S1}) + D\sin(\theta_{S1})} \tag{8}$$

where $D = -\frac{1}{2}\cos(\theta_{S1}) - \frac{\sqrt{3}}{2}\sin(\theta_{S1})$. Using this equation, the tearing strain and thus displacement from a crack can be calculated, measured by two sensors at a particular angle. Substituting back into Eq. (6) allows extraction of the isolated crack opening strain and thus displacement.

3. Turbine loading model

Following the installation, a simple model was developed to verify the integrity of the tower sensors, as explained in depth in [21]. A cantilever can be used to model the loading on a wind turbine, with overturning moment, M, caused by the addition of rotor thrust and wind distribution on tower area. Eq. (9) shows the final output from the model for estimated tower base strains, ϵ_T at sensor positions, θ_S:

$$\epsilon_T = \frac{M d_T}{2 I E_s}\cos(\alpha - \theta_S) \tag{9}$$

where $d_T = 5$ m is the tower diameter (assumed constant), $I = 2.454\ \text{m}^3$ is the second moment of inertia of the tower, $E_s = 200$ GPa is the Young's Modulus of structural steel and α is the turbine yaw. The overturning moment is calculated using Eq. (10):

$$M = \frac{1}{7}\rho V_0^2 \left(C_T(V_0) A_r H + \frac{7}{16} d_T C_{dr} H^2\right) \tag{10}$$

where $\rho = 1.225\ \text{kg/m}^3$ is the air density, $C_T(V_0) = 0$ to 0.83 is a varying quantity dependent on wind speed, V_0, unique to turbine design [29]. The area span of the rotor and blades is represented by $A_r = \pi r^2$ where $r = 54$ m is the blade length, $H = 80$ m is the height of the rotor and $C_{dr} = 0.5$ [30] is the tower drag coefficient.

The above equations concern steady-state or static conditions when the turbine is operating at rated power output, allowing disc theory to be applied [31]. Despite the wind speed dependency of C_T and M, one cannot assume the turbine operates as expected at these wind speeds. Witnessed frequently, large varying wind speeds were accompanied by constant or varying rotor speed, an example of which is shown in Fig. 7 from SCADA data. In this window, rotor speed is witnessed at both 2 rpm and 15 rpm for wind speeds varying from 5 to 25 ms^{-1}.[1] Therefore, during analysis, only time windows of rated operation and steady-state conditions are used. This provides a relatively accurate prediction for the strain in any tower sensor. Limitations of this model are described further in [21]. An example of the measured tower strain against prediction for such a window is shown in Fig. 8.

Concrete's stress-strain relationship can be expressed as non-linear overall, since micro-cracking occurs almost immediately [32]. For small load changes, however, the stress-strain relationship will appear to be linear, with only larger loads revealing the non-linearity. During early stages of monitoring, we have found that cracks show a linear response to load, or equivalently, to the strain measured in the tower:

$$\Delta L_a = J_p\, \epsilon_T \tag{11}$$

where ΔL_a and ϵ_T represent crack displacement and tower strain

[1] It is also worth noting that this particular period demonstrated the most extreme wind conditions experienced during the monitoring period.

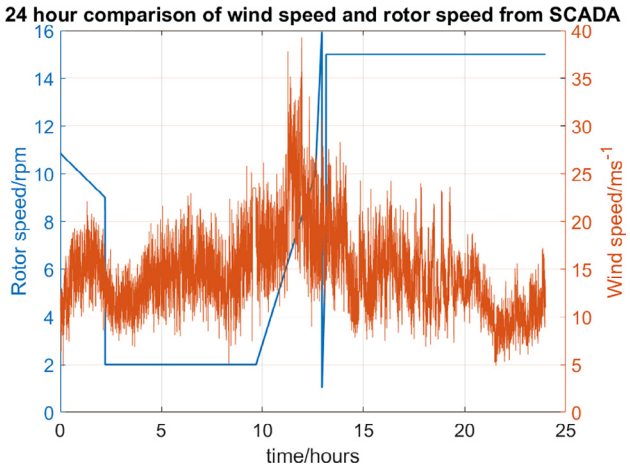

Fig. 7. Comparison of varying wind speed and rotor speed over a 24 h time period, also demonstrating the most extreme wind conditions experienced during this monitoring period.

respectively. The constant J_p for crack sensor B1 using strains from tower sensor 2 is −0.008, the magnitude of which will vary depending on crack and tower sensor being analysed as well as yaw/wind direction. An example of this linearity during an early period of monitoring is shown in Fig. 9. When using this method to extract deterioration, we also must use time windows of rated operation, as it is only during this time we know that tower strains are verified. Therefore, during these windows, ϵ_T in Eq. (11) can either be derived from SCADA data or preferably taken from tower strain sensor measurements.

4. Results

The objective of this work is to identify if the cracks monitored are displaying any visible deterioration in data over the initial 9 month period, beginning in January. To do this, an initial method was developed to identify specific types of deterioration, and will continue to be developed as further understanding of crack behaviour is gained. The first step is to define how this deterioration would manifest within crack width data. For this work, three types of deterioration have been defined: “reactive”, “permanent” and “behavioural”, and will be dis-

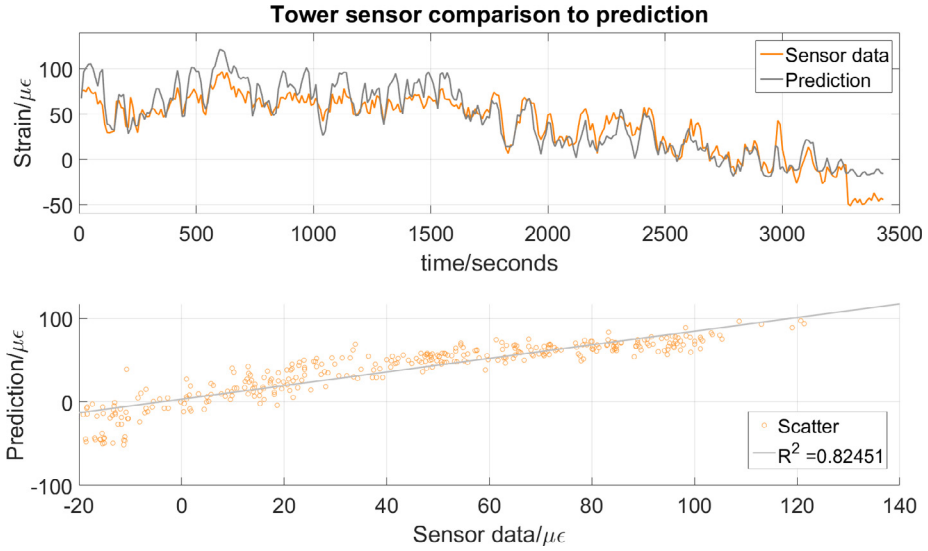

Fig. 8. Verification of tower sensor data by comparing to model prediction from SCADA data (Eq. (9)).

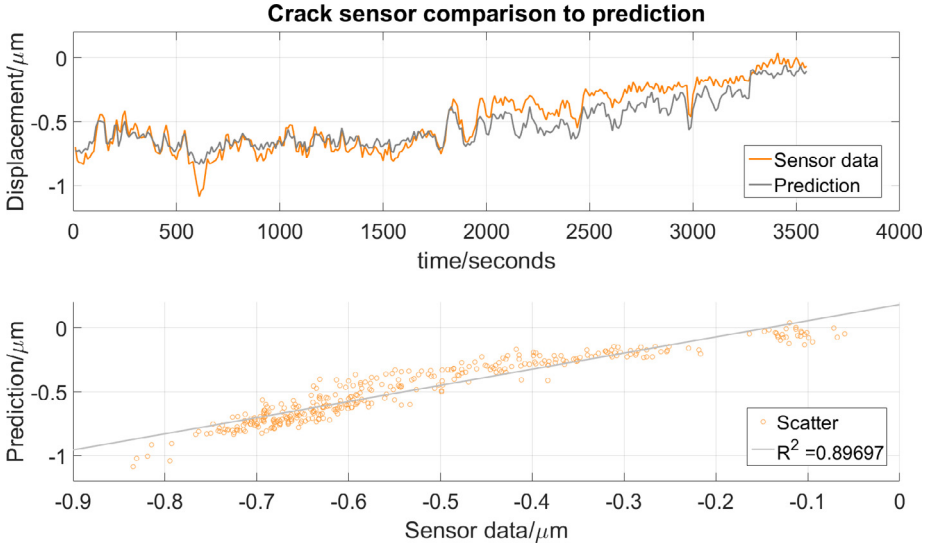

Fig. 9. Visual comparison of crack sensor data to prediction, gained by a linear relationship to tower sensor (Eq. (11)).

Table 1
Description of each deterioration.

Deterioration type	Loading	SCADA characteristics	Numerical representation
Reactive	instant large change	power transition 0 to rated	change in crack reactions to instant loads
Permanent	"dead load"	represents lowest load	change in crack "rest" width over time
Behavioural	at rated	steady-state rated	variation of R^2 from model fit

cussed in more detail in the following sections. Table 1 outlines the varying characteristics of each type. The first two can be extracted by identifying and comparing particular characteristics at two separately defined time periods. The third method uses the model described in Section 3 to determine if magnitudes and linearity of crack displacements to tower strains vary over time during rated operation.

In Fig. 3, modules B and C are labelled as these are the only two modules that were continually monitored during the initial 9 month period. As discussed, each module contains two displacement sensors, labelled: "B1", "B2", "C1" and "C2". During discussions, deterioration is compared to an estimated crack width of 0.1 mm as this is an acceptable width to the operator prior to the crack requiring repair.

4.1. Reactive

During operation, turbines undergo start-stop procedures for multiple reasons. The most frequent of which in the case of the instrumented turbine, is blade pitch lubrication, which usually occurs once every 24 h. This of course will vary for other turbine operators. Start-stop procedures also occur in this turbine during power curtailments, maintenance, cable untwisting and emergency stops. All of which cause the rotor to decelerate rapidly to a stop (or to a slower speed) for a length of time, before starting again. The rate of deceleration varies with procedure, the highest occurring during emergency stops. Start-up procedures follow, and the rotor accelerates to operational speeds. A 2.3 MW turbine power output and rotor speed from SCADA data during a blade pitch lubrication procedure is shown in Fig. 10.

This is relevant to cracks, as the turbine loads are greatest during rated conditions (or above rated, depending on blade pitch), and lowest when rotor speed is zero. Therefore, during these start-stop procedures, the turbine loads are also transitioning from maximum to minimum over an extremely short time period. Consequently, concerning blade lubrication, the foundation cracks undergo fast displacement changes every 24 h, which could potentially accelerate damage. This displacement change, or reaction, to the defined loading event may deviate over time, which could represent deterioration. For example, should a crack displacement due to the blade lubrication procedure become greater over time, one could assume that this crack is deteriorating. Fig. 11 illustrates the application of this method to module B. Two transitions,

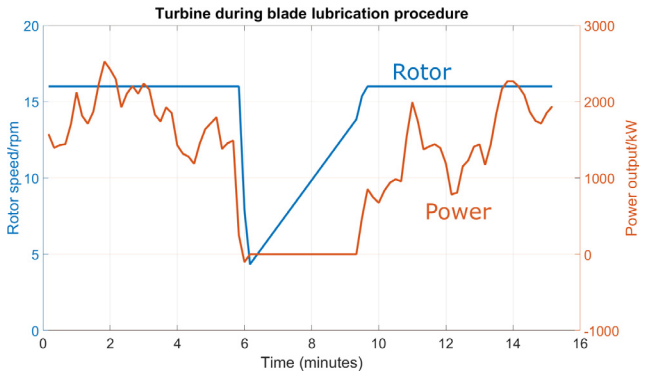

Fig. 10. Blade lubrication procedure: 2.3 MW turbine power output and rotor speed from SCADA data.

recorded in January and September, are shown with accompanying SCADA characteristics: power, rotor speed and wind speed. These values are as similar as possible, but will vary slightly. The magnitude of transitions are shown in the legend for each sensor.

The magnitude of each transition is calculated by taking the difference between means of 10 data point windows prior to and after the transition takes place. This method is applied to each sensor and results are shown in Table 2. Column 1 and 2 show the magnitude of the transition in January and September, respectively. The third column "Deterioration" is simply the value acquired by subtracting the January transition from the September transition. A positive value means the later transition either opened more or closed less than the early transition, depending on the nature of the early transition (opening or closing).

In the case of module B, the positive deterioration (column 3) represents a smaller closing transition, since the crack is closing under the chosen loading events. This could potentially mean the cracks are becoming wider as they are less susceptible to closing. Emphasis should be made on the minuscule magnitude of these crack displacements and deterioration, with the maximum displacement of $-1.3584\,\mu m$ in sensor B2 and largest deterioration of $0.4968\,\mu m$ in sensor B1. This represents <1% of the total crack width (0.1 mm) in change. Concerning the deterioration in sensor B1, at this point it is difficult to tell what the cause of this is. We simply know that later data shows this sensor reacting less severely to closing transitions. The following analysis methods may be able to determine if this is the crack, or the sensor. Since this is only evident in sensor B1, initial conclusion is that the sensor itself is the cause, perhaps due to a decrease in strain sensitivity. Module C portrays smaller reactions to these transitions, and the deterioration is equally small. Crack sensor C2 showed no reaction during the transition in September, but also displayed infrequent reactions during transitional analysis of early data. This suggests it is not an effect of deterioration during this 9 month period, rather just a characteristic of the crack. Should a crack deteriorate to a significant state, one would expect a much larger value for the deterioration, concluding that each crack measured has not shown "reactive" degradation.

4.2. Permanent

This type of deterioration represents the overall crack width change over time. To accurately extract this information, a "zero load" (known in the industry as "dead load") state is required. "Dead load" refers to periods when the only loading on the structure is from the weight of the structure itself. This means wind speed, power, and rotor speed equalling approximately zero, with yaw remaining constant. One other consideration includes the blade pitch which, depending on the current yaw position, can cause varying crack widths, thus ensuring these values are constant is essential. Load on the turbine is continually changing since wind speed is rarely constant for long periods of time. Therefore, windows as close to this "dead load" requirement as possible are extracted from two time points - one early and one late during the measurement period. The mean of crack widths are then compared. Applying this method to each sensor gains the results shown in Table 3. Column 1 and 2 show the crack widths in January and October respectively, with column 3 portraying the change in crack width.

At first glance, the negative deterioration suggests each crack has closed gradually over time. Emphasis is again made on the minuscule

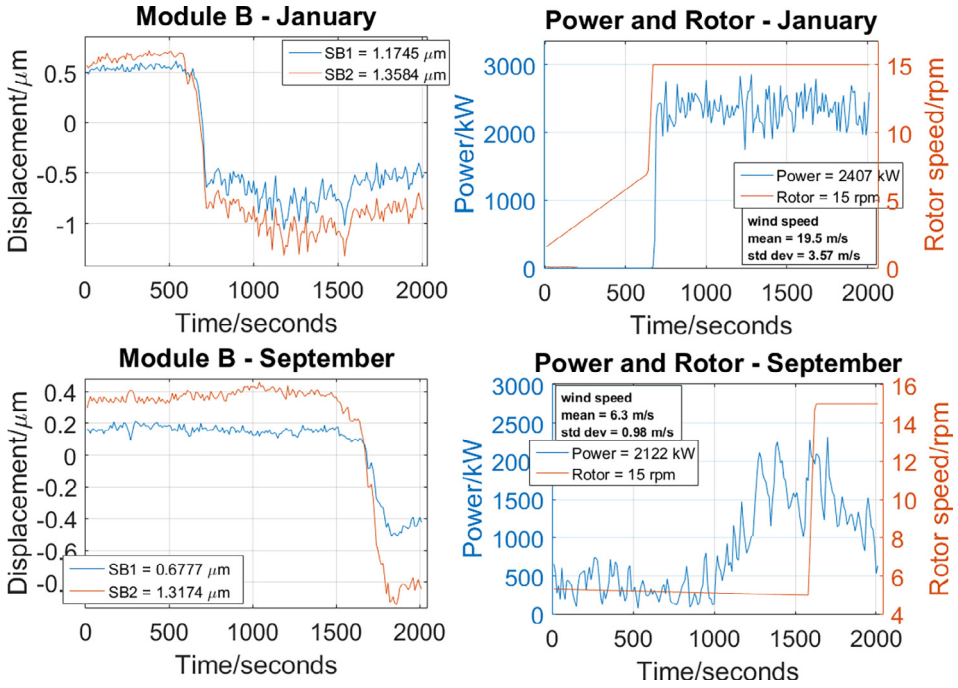

Fig. 11. Reaction to instant load: comparison of module B during loading events in January and September with similar characteristics.

Table 2
"Reactive" deterioration in each sensor, determined by the change in transition under similar loading at separate time points.

Sensor	Jan. ΔY_J (μm)	Sep. ΔY_S (μm)	Deterioration $\Delta Y_S - \Delta Y_J$ (μm)
B1	−1.1745	−0.6777	0.4968
B2	−1.3584	−1.3174	0.0410
C1	0.1199	0.1183	−0.0017
C2	0.0838	0	−0.0839

Table 3
"Permanent" deterioration in each sensor, determined by taking the mean of a short window under "dead load" conditions.

Sensor	Jan. Y_J (μm)	Oct. Y_O (μm)	Deterioration $Y_O - Y_J$ (μm)
B1	0.4474	0.0277	−0.4197
B2	0.6573	0.0425	−0.6148
C1	−0.0282	−0.0228	−0.0054
C2	−0.0271	−0.0222	−0.0049

scale of these changes, with the maximum decrease of 0.6148 μm, again <1% of an estimated total crack width (0.1 mm). Unlike "reactive" deterioration, which concerns instant changes, this deterioration has larger susceptibility to uncertainties such as temperature compensation errors (drifts) or sensor degradation. It is possible that this gradual closing is evidence of such an affect. Should the crack widths significantly change, this would be identified by the "permanent" method.

4.3. Behavioural

"Behavioural" deterioration encompasses everything that has not already been mentioned. This has been named as such since it represents any changes in how the crack behaves in response to loading. It has been assumed that if the cracks are at an early damage state, they will have an equivalent magnitude to previous states and behave linearly to tower strains, as explained in Section 3. Therefore, during analysis we should look for non-linearity, magnitude change and also for changing direction (predicted tension accompanied by crack compression) which could also be evidence of deterioration occurring. The prediction model discussed in Section 3 is used to both extract periods of verified tower strains and to produce an expected linear crack behaviour for both early and late time periods, which is then compared to the real data. The value for constant J_p (-0.008) for each sensor is unchanged, so any magnitude changes can also be extracted. For this analysis, an entire month of data was processed and the window with greatest R^2 is presented.

Fig. 12 shows two plots, one in January and the other September, of sensors B1 and B2 against the prediction (Eq. (11)) of the crack displacement. Tower sensor strains for ϵ_T have been used, but only during windows where the prediction from Eq. (9) has a high correlation to the data. In the legend, the R^2 value is provided for the prediction fit to each sensor (B1/B2). It is clear that in January, both sensors and prediction are very closely related, with an R^2 of ≈ 90%. This leads us to believe that the cracks are superficial during the early stages, as expected, as they relate linearly to the tower strains. In September, we also see a high R^2 value, suggesting the cracks are continuing to relate linearly to tower strains. However, it is clear that sensor B1 has significantly decreased in magnitude when compared to both B2 and prediction. This could be due to a few reasons. Firstly the sensor itself (B1) could be degrading, causing a decrease in strain sensitivity, K_ϵ (Eq. (1)). Secondly, from Fig. 4 we see that each sensor is measuring a single crack at a different location; therefore, perhaps the crack could be behaving differently at each location. In other words, degradation at the location of sensor B1 could be greater than at B2. Finally, there is the lateral or tearing displacements to take into account, which could also affect the overall crack displacement (Eq. (3)). In the case of sensor sensitivity decreasing, we would expect R^2 to be unchanged, as R^2 is only affected by variability and not scale. To expand on this, scaling measurements from B1 up to a magnitude equivalent to B2 would not change the value of R^2. Any reduction in K_ϵ in Eq. (1) would similarly not affect the R^2 value, as long as final displacements are greater than interrogator resolution. The documented resolution of the interrogator is 0.5 pm, which provides an approximate perfect displacement resolution of ≈ 0.032 μm. In this case, the measurements are very close, but greater than this limit; therefore, this decrease in magnitude could possibly be caused by sensor degradation. This result is consistent with the decrease in displacement found in sensor B1 from the previous

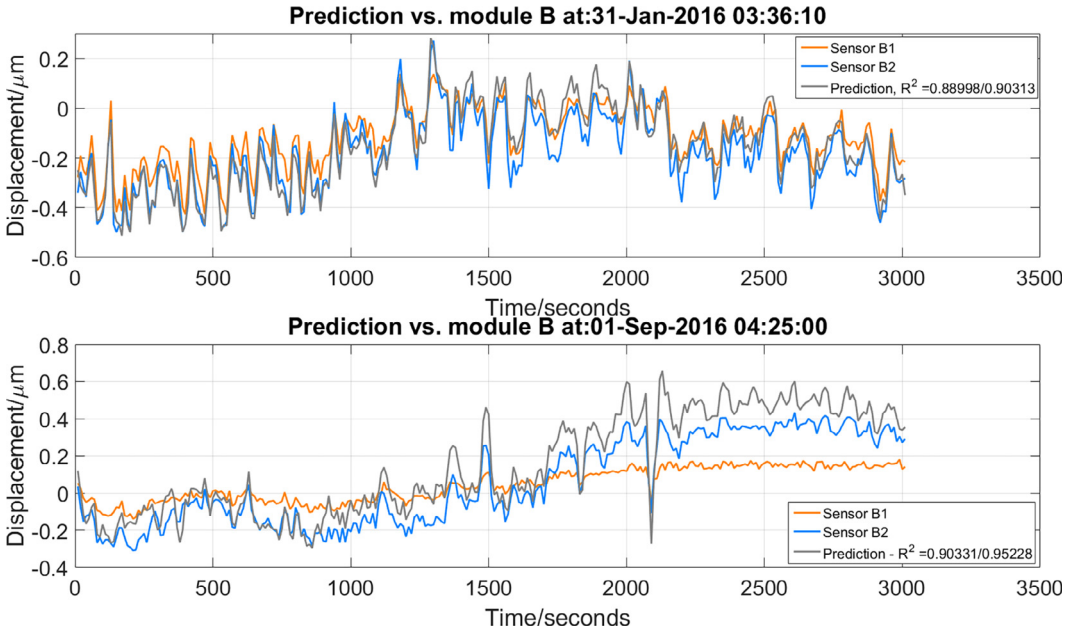

Fig. 12. "Behavioural" analysis using prediction model for crack module B.

"reactive" analysis, but not B2.

Fig. 13 applies the same method to sensor module C. In this case we see that the R^2 value has remained >0.8, suggesting no deterioration in this crack. However, we can see visibly that there is again a reduction in magnitude when comparing the sensors to the prediction, which could also be a reduction in sensitivity K_ϵ. In this case it is again not large enough to be masked by insufficient resolution.

4.4. Lateral crack movements

Explained in the installation report [21] and in Section 2.3, lateral, or tearing, crack movement can be measured using the bespoke sensor design in this work. Eq. (8) can be implemented to extract the exact amount of tearing displacement. In general, a large tearing displacement will be signified by a major difference between arm measurements. However, it was determined in the previous section that there could be evidence of a decreased strain sensitivity in only one arm. This makes tearing displacements more difficult to extract. However, we can use the prediction from the previous section to aid in the extraction. This would be represented by a prediction that was less in magnitude than one sensor arm, but greater than the another, with a large correlation (R^2) to both. This would mean either there are tearing displacements evident, or that the crack is behaving differently at each location, which is more unlikely. Unfortunately, at this point there has been no evidence of this behaviour during the "behavioural" detection method, suggesting lateral movement is non-existent during these rated power windows.

One method to quickly determine if any lateral movement is apparent over a large window of data (one month, in this case) is to simply plot a scatter graph of each sensor module. Visually, to extract tearing crack displacement, we identify any non-linear outliers that are present. Figs. 14 and 15 are scatter graphs of module B and C

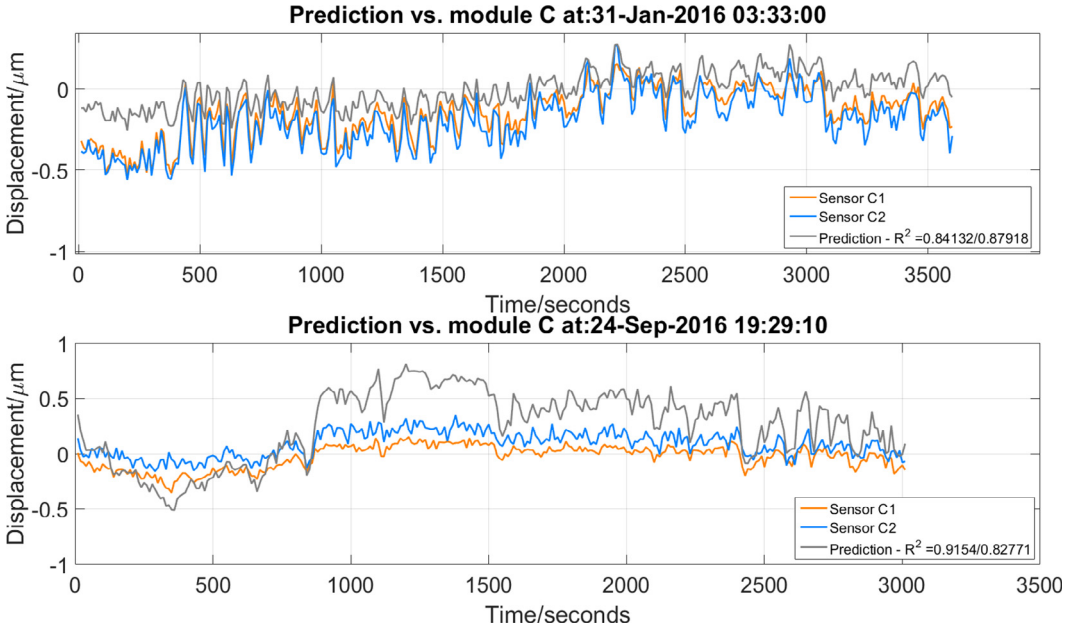

Fig. 13. "Behavioural" analysis using prediction model for crack module C.

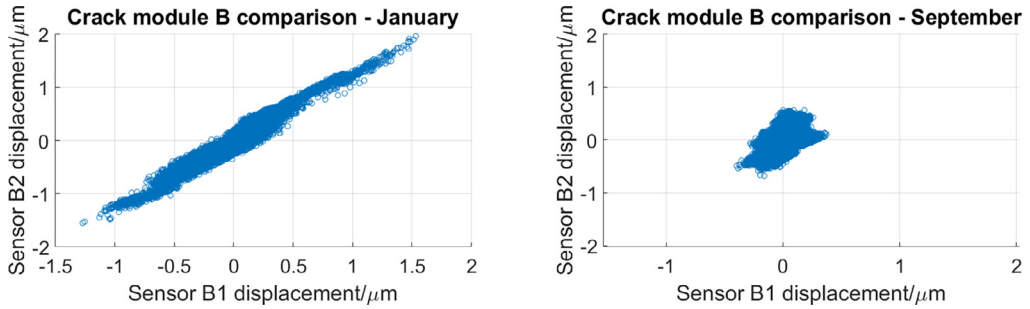

Fig. 14. Scatter graphs of each module B arm during early and late dates.

respectively for both January and September.

Firstly, from Fig. 14 of module B, we see the decrease in sensitivity that was mentioned previously. The distribution has decreased, more so in sensor B1, but remains mainly linear. We also see no outliers which would signify tearing in this crack, therefore tearing is not occurring. Analysing module C in Fig. 15, we do see some outliers highlighted by red ellipses, more dense in January. In this case sensor C1 is showing a displacement of around −0.3 μm when C2 shows + 0.2 μm. This difference occurs during a stop transition, as shown in Fig. 16 at ≈277 min. Perhaps during this instantaneous loading the crack undergoes a tearing as well, causing this difference. However, this displacement is very small and cannot be defined confidently as tearing. In future, this method could be used to identify if any major tearing displacements are occurring over a long time window.

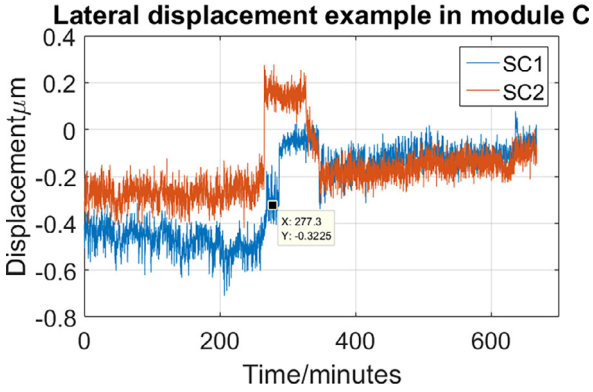

Fig. 16. Short window of tearing displacement during transition in module C.

5. Discussion

In this paper, data analysis methods for identifying crack deterioration in onshore wind turbine foundations is proposed. Three types of deterioration have been defined with extraction methods applied for the first 9 months of in situ foundation monitoring. From these methods, we can conclude that the cracks remain superficial and have not significantly deteriorated.“Reactive” deterioration is the first type, and identifies variation in crack reaction to defined loading events, caused by turbine start-stop procedures. Transitions were found to be small in magnitude, but frequent and instant, portraying a possible accelerant of deterioration. Over the initial 9 month period, the maximum “deterioration”, or largest change in reaction, was 0.4968 μm, witnessed by sensor B1. This deterioration represented a smaller closing of the crack, implying the crack could be less susceptible to closing and therefore could be degrading. This is small however, at <1% of the overall crack width (0.1 mm). Causes of this decrease are difficult to determine using this method as it simply provides a numerical value of change in magnitude to an instant load.

The second method isolated the overall crack width by analysing periods of approximately zero loading. Interestingly, results showed all cracks closing, with the maximum magnitude of 0.6148 μm shown in sensor B2. This change could potentially be explained by temperature compensation drifts or sensor degradation, as it is not expected for cracks to close over time. The gradual nature of this deterioration when compared to “reactive” means it is more susceptible to these errors. Furthermore, the approximate “dead load” state at each time-point contained differing wind speeds, which incident on the tower will cause different loads. One thing to note: this permanent deterioration is indistinguishable from new discontinuities (W_c from Eq. (2)), however, it is not expected for these to be large.

The final method compared a pre-defined prediction of crack displacements, linear to tower strains, and sensor data over short windows in January and September. Cracks are expected to behave linearly to tower strains if they are low damage or superficial. Linear behaviour was witnessed in all sensors during both windows, with a numerical representation of fit (R^2) of >88% for module B and >82% for module C. Results from this model showed that sensor B1 may have undergone sensitivity reduction, lowering measured displacement magnitudes close to the range of interrogator resolution. Sensor B2 continues to provide similar measurements to the prediction. Both sensors in module C maintained linearity to tower strains, but at a small decrease in sensitivity. This method provided greater insight into the causes of the decreases found in the previous methods as the R^2 is not affected by scale, only variability.

Lateral or tearing crack displacements can be measured with the

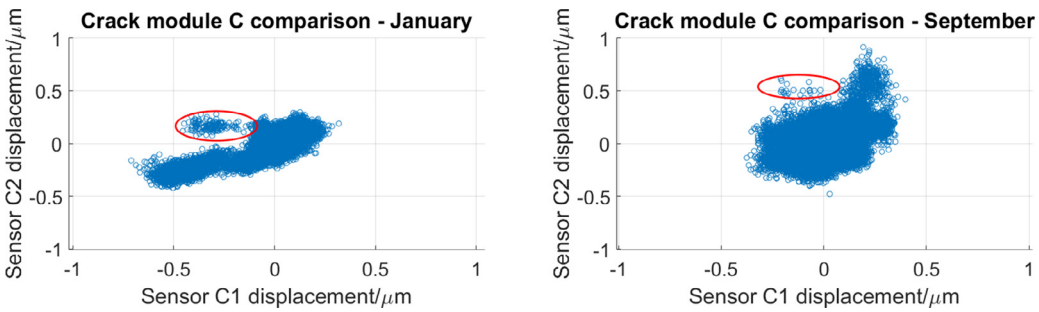

Fig. 15. Scatter graphs of each module C arm during early and late dates. Outliers are highlighted by red ellipses.

bespoke sensor design in this work if they are large. To determine if any major tearing is occurring, we can simply plot scatter graphs of each module arm and extract any non-linear outliers. Module B showed no signs of tearing, but provided further evidence as to the decreased sensitivity. Module C showed some evidence of tearing displacements, mainly during January, where one arm measured −0.3 μm and the other 0.2 μm. After extraction, this window was determined to have occurred during a stop procedure, implying tearing may be more prominent during transitions.

As discussed, turbine operators witnessed openings in these types of cracks during manual inspections prior to any sensor installation. The length of time between these inspections is unknown, but the periodic nature of manual inspections means the true time taken for cracks to degrade is unknown. Therefore, it is possible cracks during this period are not expected to deteriorate, and are at an early development stage. Therefore measurement of these crack widths will continue in order to monitor deterioration should it occur. Future work will also include improvement of the model prediction equation by including further terms such as torque, allowing more windows to be analysed. The current model is restricted to very specific operating conditions which rarely occur. These methods will continue to be applied and improved to determine if the cracks monitored deteriorate significantly. Information could also be used to inform an economic model to determine the optimal time to repair. Since, to the authors knowledge, no other onshore wind turbine foundation cracks of this nature have been monitored during operating conditions, there is no baseline for comparison. We have to assume the cracks are superficial at the early stages of monitoring and that any deviations from this is deterioration. In future, lab experiments of fatigue loading occurring to cracks using similar sensors could provide confirmation as to whether these changes are in fact due to crack deterioration. Also, it would provide a more in depth view of the nature of the crack degradation, whether it is linear or non-linear. Some evidence has been found to indicate sensors may have degraded in sensitivity, the cause of which is unknown at this point. Sensors have undergone alternating temperatures and humidities, which are the first culprits of degradation. Testing and improvements will be made to ensure this does not occur in any future installations. If such installations are undertaken, the cracks monitored should be of a much more damaged state than those measured in this work. This would increase the probability that major deterioration is present and allow for comparisons to this work. Finally, until this point only static loading and displacements have been analysed. It is possible that dynamic oscillations cause cracks to deteriorate, therefore this will also be investigated. Particularly, any oscillations occurring immediately following a transition, as it is expected these start-stop procedures are the most likely aggravation to the cracks.

6. Conclusion

Presented in this paper is an approach to determine and characterise deterioration of cracks that are present in onshore wind turbine foundations. Cracks have been previously instrumented with FBG based long-gauge strain sensors. Analysis presented in this work considers the first 9 months of monitoring. Three types of deterioration and methods to extract them have been defined and applied to the in situ sensors monitoring crack displacements. Results show that there are very minor differences between crack displacements during early and late monitoring windows. From these results, we determine that the monitored cracks have not significantly deteriorated, and therefore remain superficial.

Acknowledgments

This work was supported by ScottishPower Renewables, SSE and the Engineering and Physical Sciences Research Council, Grant No. EP/G037728/1.**Data statement**

Due to commercial restrictions, data underpinning this publication cannot be made openly available. Further information about the data and conditions for access are available from the University of Strathclyde KnowledgeBase at http://dx.doi.org/10.15129/6d1ad9e3-b78d-4d55-bfc0-d958abbb94ab.

Appendix A. Supplementary material

Supplementary data associated with this article can be found, in the online version, at http://dx.doi.org/10.1016/j.engstruct.2018.04.003.

References

[1] G.W.E. Council. Global wind report; 2016. < http://www.gwec.net/publications/global-wind-report-2/ > .
[2] I.R.E. Agency. Renewable capacity statistics 2017; 2017. < http://www.irena.org/ > .
[3] Barszcz T, Randall R. Application of spectral kurtosis for detection of a tooth crack in the planetary gear of a wind turbine. Mech Syst Signal Process 2008;23(4):1352–65.
[4] Reder MD, Gonzalez E, Melero JJ. Wind turbine failures – tackling current problems in failure data analysis. J Phys: Conf Ser 753. http://dx.doi.org/10.1088/1742-6596/753/7/072027. http://iopscience.iop.org/1742-6596/753/7/072027.
[5] Loraux C, Brühwiler E. The use of long term monitoring data for the extension of the service duration of existing wind turbine support structures. J Phys: Conf Ser 753. http://dx.doi.org/10.1088/1742-6596/753/7/072023. http://iopscience.iop.org/1742-6596/753/7/072023.
[6] Taylor SG, Farinholt K, Choi M, Jeong H, Jang J, Park G, et al. Incipient crack detection in a composite wind turbine rotor blade. J Intell Mater Syst Struct 2014;25(5):613–20. http://dx.doi.org/10.1177/1045389X13510788.
[7] Brownjohn JMW, Bocciolone M, Curami A, Falco M, Zasso A. Humber bridge full-scale measurement campaigns 1990-1991. J Wind Eng Ind Aerodyn 1994;52(C):185–218. http://dx.doi.org/10.1016/0167-6105(94)90047-7.
[8] Ko JM, Ni YQ. Structural health monitoring and intelligent vibration control of cable-supported bridges: research and application. KSCE J Civ Eng 7(6):701–16. http://dx.doi.org/10.1007/BF02829139.
[9] Ko JM, Ni YQ. Technology developments in structural health monitoring of large-scale bridges. Eng Struct 2005;27(12 SPEC. ISS.):1715–25. http://dx.doi.org/10.1016/j.engstruct.2005.02.021.
[10] Inaudi D, Glisic B. Distributed fiber optic strain and temperature sensing for structural health monitoring. In: Proceedings of the IABMAS 6.
[11] Nicolas MJ, Sullivan RW, Richards WL. Large scale applications using FBG sensors: determination of in-flight loads and shape of a composite aircraft wing. Aerospace 2016;3(3):18.
[12] Adachi Y. Monitoring technologies for maintenance and management of urban highways in Japan. In: Conference proceedings: sensing issues in civil structural health monitoring. http://dx.doi.org/10.1007/1-4020-3661-2_2.
[13] Sigurdardottir DH, Glisic B. On-site validation of fiber-optic methods for structural health monitoring: Streicker bridge. J Civ Struct Health Monit 2015;5(4):529–49. http://dx.doi.org/10.1007/s13349-015-0123-x.
[14] He K, Zhu W. Structural damage detection using changes in natural frequencies: theory and applications. J Phys Conf Ser 305. http://dx.doi.org/10.1088/1742-6596/305/1/012054.
[15] Lee E, Rahmatalla S, Eun H. Damage detection by mixed measurements using accelerometers and strain gages, Smart Mater Struct 22. http://dx.doi.org/10.1088/0964-1726/22/7/075014.
[16] Currie M, Saafi M, Tachtatzis C, Quail F. Structural integrity monitoring of onshore wind turbine concrete foundations. Renew Energy 2015;83:1131–8. http://dx.doi.org/10.1016/j.renene.2015.05.006.
[17] Rao Y. In-fibre Bragg grating sensors. Meas Sci Technol 1997;8(4):355–75. http://dx.doi.org/10.1088/0957-0233/8/4/002.
[18] Kashyap R. Fibre Bragg gratings, 2nd ed.; 2010.
[19] Niewczas P, Fusiek G. Induction heated assisted optical fibre bonding and sealing technique. In: 21st international conference on optical fiber sensors, vol. 7753; 2011. p. 77536H–77536H-4. http://dx.doi.org/10.1117/12.885942.
[20] Chan THT, Yu L, Tam HY, Ni YQ, Liu SY, Chung WH, et al. Fiber Bragg grating sensors for structural health monitoring of Tsing Ma bridge: background and experimental observation. Eng Struct 2006;28(5):648–59. http://dx.doi.org/10.1016/j.engstruct.2005.09.018.
[21] Perry M, McAlorum J, Fusiek G, Niewczas P, McKeeman I, Rubert T. Crack monitoring of operational wind turbine foundations. Sensors 2017;17:1925. http://dx.doi.org/10.3390/s17081925.
[22] Hill KO, Meltz G. Fiber Bragg grating technology fundamentals and overview. J Lightwave Technol 15(8). http://dx.doi.org/10.1109/50.618320.
[23] Orr P, Niewczas P, Dyśko A, Booth C. FBG-based fibre-optic current sensors for power systems protection: laboratory evaluation. In: Universities Power Engineering Conference (UPEC).
[24] Perry M, Saafi M, Fusiek G, Niewczas P. Hybrid optical-fibre/geopolymer sensors for structural health monitoring of concrete structures. Smart Mater Struct 24.
[25] Audenaert K, Schutter GD, Marsavina L, Boel V. Influence of cracks and crack width on penetration depth of chlorides in concrete. Eur J Environ Civ Eng interrefdoi:10.1080/19648189.2009.9693134httphttps://doi.org/10.1080/19648189.2009.

9693134.
[26] Irwin GR, Kies JA. Critical energy rate analysis of fracture strength. Weld J Res Suppl. 33:193s–8s.
[27] Glisic B. Influence of the gauge length on the accuracy of long-gauge sensors employed in monitoring of prismatic beams. Meas Sci Technol 2011;22(3):35206. http://dx.doi.org/10.1088/0957-0233/22/3/035206.
[28] Zehnder AT. Fracture mechanics 62. http://dx.doi.org/10.1007/978-94-007-2595-9.
[29] Montavon C, Jones I, Staples C, Strachan C, Gutierrez I. Practical issues in the use of CFD for modelling wind farms. In: European wind energy conference.
[30] Kono T, Nebucho S, Kogaki T, Kiwata T, Kimura S, Komatsu N. Numerical analysis of the effects of rotating wind turbine blades on the aerodynamic forces acting on tower. Energies 10:121.
[31] Burton T, Jenkins N, Sharpe D, Bossanyi E. Wind energy handbook. 2nd ed. Wiley; 2011.
[32] B. Standard, Steel, concrete and composite bridges, bs 5400-4:1990.